Deformation of the Normal Monkey Optic Nerve Head Connective Tissue after Acute IOP Elevation within 3-D Histomorphometric Reconstructions

Hongli Yang,[1,2,3] *J. Crawford Downs,*[2,3] *Ian A. Sigal,*[2,3] *Michael D. Roberts,*[3] *Hilary Thompson,*[4] *and Claude F. Burgoyne*[1,2]

Purpose. To characterize optic nerve head (ONH) connective tissue deformation after acute (15 or 30 minutes) intraocular pressure (IOP) elevation in six adult normal monkeys using three-dimensional (3-D) histomorphometry.

Methods. Trephined ONH and peripapillary sclera from both eyes of six monkeys, each perfusion fixed with one eye at IOP 10 mm Hg (IOP-10) and the other at IOP 30 or 45 mm Hg (IOP-30 or IOP-45, by anterior chamber manometer), were serially sectioned, 3-D reconstructed, 3-D delineated, and quantified according to standard parameters. For each monkey, intereye differences (high-IOP eye minus IOP-10) for each parameter were calculated and compared by ANOVA and EPID*max* both overall and regionally. EPID*max* deformations for each parameter were defined to be those statistically significant differences that *exceeded the maximum physiologic intereye difference* within six bilaterally normal monkeys in a previous report.

Results. Regional EPID*max* laminar thinning, posterior bowing of the peripapillary sclera, and thinning and expansion of the scleral canal were present in most high-IOP eyes and were colocalized in those demonstrating the most deformation. Laminar deformation was minimal, not only posteriorly but in some cases anteriorly in the high-IOP eyes. No increase in deformation was seen in the IOP-45 versus the IOP-30 eyes.

Conclusions. ONH connective tissue alterations after acute IOP elevation involve regional thinning, stretching, and deformation of the lamina cribrosa and peripapillary sclera that are minimal to modest in magnitude. The time-dependent character of these alterations and their compressive, expansile, and shear effects on the axons, the astrocytes, and the laminar and posterior ciliary circulations remain to be determined. (*Invest Ophthalmol Vis Sci.* 2009;50:5785–5799) DOI:10.1167/iovs.09-3410

The neural, vascular, and connective tissues of the optic nerve head (ONH) make up a dynamic environment wherein 1.2 to 2.0 million retinal ganglion cell (RGC) axons converge, turn, and exit the eye through the neural canal opening (NCO; see Figs. 2, 7). Within the scleral portion of the neural canal, the bundled axons pass through the lamina cribrosa, a three-dimensional (3-D) meshwork of astrocyte-covered, capillary-containing connective tissue beams. Although glaucomatous damage to the visual system most likely causes major pathophysiologic changes within the RGC body,[1–6] photoreceptors,[7–11] lateral geniculate body,[12–14] and visual cortex,[14] strong evidence suggests that damage to the retinal ganglion cell axons within the lamina cribrosa of the ONH[15–20] is the central pathophysiology underlying glaucomatous vision loss. Recent studies in humans,[21,22] monkeys,[19,20,23–28] rats,[29–31] and mice,[32] support the importance of the ONH by describing significant alterations within the prelaminar, laminar, and peripapillary scleral tissue of the ONH at the earliest detectable stage of experimental glaucoma. Although the interaction between ONH connective tissue deformation,[19,20,24,26,33] altered astrocyte function,[34–38] and ischemia[39–42] are beginning to be elucidated, the multifactorial insults to the RGC axons remain to be characterized. These insults may include intraocular pressure (IOP)–related[27] and non–IOP-related components[43–46] that are not dependent on IOP-induced connective tissue deformation, damage, and/or remodeling.

The ONH has been characterized as a biomechanical structure in studies of the deformation of the lamina cribrosa after acute IOP elevations in cadaveric eyes[21,22,47] and in monkeys.[19,48] Levy and Crapps[22] reported a 12-μm average posterior (outward) movement of the central lamina with acute IOP elevations from 10 to 25 mm Hg for short periods in cadaveric eyes. Yan et al.[21] found that increasing IOP from 5 to 50 mm Hg for 24 hours produces an average posterior deformation of the central lamina of 79 μm and slight contractions of the scleral canal and thinning of the lamina that do not achieve significance.

We have studied acute IOP-induced deformation of the monkey ONH connective tissues by using two-dimensional (2-D) histomorphometry within two groups of monkey eyes.[19,48] In the first study, Bellezza et al. [48] demonstrated that the laminar position was significantly more anterior (toward Bruch's membrane), the lamina cribrosa was thinner, and the scleral canal diameter was larger in a group of monkey eyes that had been perfusion fixed at IOP 10 mm Hg (IOP-10) compared with a group of immersion fixed (IOP-0) eyes. Their results suggest that the lamina cribrosa and scleral canal wall act like an expandable trampoline at low levels of IOP, with the canal expanding and the lamina thinning and becoming more tautly stretched as IOP is elevated from 0 to 10 mm Hg.

From the [1]Optic Nerve Head Research Laboratory and the [3]Ocular Biomechanics Laboratory, Devers Eye Institute, Legacy Health System, Portland, Oregon; the [2]Department of Biomedical Engineering, Tulane University, New Orleans, Louisiana; and the [4]School of Public Health, Louisiana State University Health Sciences Center, New Orleans, Louisiana.

Supported by USPHS Grant R01EY011610 (CFB) from the National Eye Institute, National Institutes of Health, Bethesda, Maryland; a grant from the American Health Assistance Foundation, Rockville, Maryland (CFB); a grant from The Whitaker Foundation, Arlington, Virginia (CFB); a Career Development Award (CFB); The Legacy Good Samaritan Foundation, Portland, Oregon; and the Sears Trust for Biomedical Research, Mexico, Missouri.

Submitted for publication January 14, 2009; revised May 29, 2009; accepted September 1, 2009.

Disclosure: **H. Yang**, None; **J.C. Downs**, None; **I.A. Sigal**, None; **M.D. Roberts**, None; **H. Thompson**, None; **C.F. Burgoyne**, None

The publication costs of this article were defrayed in part by page charge payment. This article must therefore be marked "*advertisement*" in accordance with 18 U.S.C. §1734 solely to indicate this fact.

Corresponding author: Claude F. Burgoyne, Optic Nerve Head Research Laboratory, Devers Eye Institute, 1225 NE 2nd Avenue, PO Box 3950, Portland OR 97208-3950; cfburgoyne@deverseye.org.

In a subsequent study,[19] normal young adult monkeys were perfusion fixed 15 to 80 minutes after one eye was set to 10 mm Hg and the other to 30 or 45 mm Hg by an anterior chamber manometer. This study demonstrated an overall posterior laminar deformation of 10 to 23 μm in the high-IOP eyes relative to the contralateral IOP-10 control eyes. However, this deformation did not exceed the magnitude of intereye differences in laminar surface position in a separate group of bilaterally normal monkey eyes immersion fixed after enucleation.

The results of these human and monkey studies, considered together, suggest that the lamina cribrosa and scleral canal wall deform after acute IOP elevation in normal monkey and human eyes, that the deformation of the lamina may be anterior rather than posterior within the canal, and that this deformation may increase as the period of IOP elevation is extended. However, the measurements in most of these studies were taken from 2-D histologic sections and were therefore subject to artifacts introduced by the section angle through the tissue, section distortion during mounting, and the lack of a consistent reference plane for measurements, all of which may have limited their accuracy. Levy and Crapps[22] used 2-D x-ray images and also had artifacts induced by the angle of imaging and the uncertain position of the platinum wire relative to the anterior lamina cribrosa surface.

Although we have emphasized that IOP-related axonal trauma within the lamina cribrosa may be unrelated to actual connective tissue deformation,[25,33] it remains important to identify the biomechanical determinants of laminar and peripapillary scleral displacement at a given IOP. The purpose of this study was to characterize connective tissue deformation of the lamina, scleral canal wall, and peripapillary sclera within 3-D ONH reconstructions after acute (15 or 30 minutes) IOP elevation (from 10 mm Hg to 30 or 45 mm Hg) in six young adult normal monkeys, by using 3-D histomorphometry.[24–26,28]

Materials and Methods

Animals

All animals were treated in accordance with the ARVO Statement for the Use of Animals in Ophthalmic and Vision Research. One female and five male normal monkeys (aged 5–14 years) were used (Table 1). Before they were killed, IOP and axial length were measured in both eyes of each animal on three to five separate occasions. IOP was defined to be the mean of three measurements by handheld tonometer (Tono-Pen XL; Bio-Rad, Glendale, CA). Axial length was defined to be the mean of the longest 3 of 10 ultrasonic axial length measurements (model A1500; Sonomed, Lake Success, NY).

Monkey Euthanatization and Perfusion Fixation at Prescribed IOP

Both eyes of each monkey were cannulated with a 27-gauge needle with the monkey under deep pentobarbital anesthesia, and the IOP was set to 10 mm Hg with an adjustable saline reservoir. After a minimum of 30 minutes, IOP was raised to either 30 or 45 mm Hg in one eye (IOP-30 and IOP-45, respectively) for 15 minutes (30 minutes in monkey 6) and the monkey was perfusion fixed via the descending aorta with 1 L of 4% buffered hypertonic paraformaldehyde solution followed by 6 L of 5% buffered hypertonic glutaraldehyde solution pressurized during perfusion to approximately 4 psi in five monkeys, and 15 psi in one monkey (monkey 1, the only monkey in which perfusion pressure was monitored via the brachial artery during perfusion). After perfusion, IOP was maintained for 1 hour, and then each eye was enucleated, all extraocular tissues were removed, and the intact anterior chamber was excised 2 to 3 mm posterior to the limbus. By gross inspection, perfusion was excellent in all six IOP-10 eyes. However, blood was variably present in the retinal vessels, posterior

Table 1. Animal and Eye Data

No.	ID	Weight (kg)	Age (y)	Species	Sex	Eye	IOP (mm Hg)*	Fixation Pressure (mm Hg)	Axial Length (mm)	Duration of IOP Elevation (min)	Number of Serial Section Images	Histomorphometric Optic Disc Size†		
												Vertical (μm)‡	Horizontal (μm)§	Area (mm^2)‖
1	20852	4.32	14	Rhesus	Female	R	11	45	NA	15	686	1214	869	0.828
						L	11	10	NA		554	1216	864	0.825
2	5889	5.9	6	Rhesus	Male	R	9	45	20.51	15	316	1415	1042	1.158
						L	8	10	20.2		349	1384	1009	1.097
3	7484	5.9	5	Rhesus	Male	R	9	45	21.39	15	283	1641	1143	1.473
						L	8	10	21.02		306	1577	1131	1.401
4	AA3P	5.5	9	Cynomolgus	Male	R	12	30	18.49	15	325	1238	828	0.805
						L	12	10	18.29		290	1263	808	0.801
5	278	6.0	5	Rhesus	Male	R	4	30	19.85	15	217	1534	1112	1.340
						L	4	10	19.6		170	1487	1073	1.253
6	528	7.2	6	Rhesus	Male	R	11	30	19.89	30	280	1368	999	1.074
						L	11	10	18.54		265	1318	914	0.946

* Mean IOP of all $n = 3$ to 9 baseline measurements in monkeys under ketamine/xylazine anesthesia.
† Optic disc dimension, as determined by the clinically visible optic disc margin, which is the NCO in these monkey eyes at the perfusion pressure indicated.
‡ Vertical length, as determined by the major length of the NCO ellipse.
§ Horizontal length, as determined by the minor length of the NCO ellipse.
‖ Disc area is determined by the area of the NCO ellipse.

ciliary arteries, and vortex veins of the six high-IOP eyes. The posterior scleral shell with intact ONH, choroid, and retina were placed in 5% glutaraldehyde solution for storage.

Generation of the Aligned Serial Section Images for Each ONH and 3-D ONH Reconstruction

These steps have been described in detail in our previous reports.[20,24] Briefly, the ONH and peripapillary sclera were trephined (6-mm diameter), pierced with alignment sutures, embedded in paraffin, mounted on a microtome, and sectioned. After each section was cut, the block surface was stained with a 1:1 (vol/vol) mixture of Ponceau S and acid fuchsin stains and then imaged at a resolution of 2.5 × 2.5 μm per pixel. The sections were serially cut at 3.0-μm thickness, and the staining and imaging process was repeated after each cut. Imaging began at the vitreoretinal interface and continued ~200 μm into the retrolaminar orbital optic nerve.

Serial section images of the ONH were aligned in the anterior-to-posterior direction and stacked at 3.0-μm intervals into a 3-D reconstruction of the ONH and peripapillary scleral connective tissue (~1080 × 1520 × 400 voxels, each 2.5 × 2.5 × 3.0 μm in size).

3-D Delineation of ONH and Peripapillary Scleral Landmark Points

Our 3-D delineation technique has been described in detail in previous reports[24–26] (see Fig. 1). Briefly, with the use of the custom software (based on the Visualization Toolkit, Clifton Park, NY), 3-D ONH reconstruction was loaded and the delineator designated the approximate center of the neural canal as the center of rotation, around which 40, 7-voxel-thick, digital, radial, sagittal slices of the 3-D reconstruction were serially served at 4.5° intervals to the delineator's workstation (Fig. 1A).

Within each sagittal section image, the delineator marked seven structures—the lamina cribrosa, sclera, neural boundary, Bruch's membrane (BM), internal limiting membrane (ILM), central retinal vessels, and subarachnoid space—and six pairs of neural canal landmark points—the NCO which in the monkey is most often the innermost extension of the Bruch's membrane opening (BMO), the anterior scleral canal opening (ASCO), the anterior laminar insertion (ALI), the posterior laminar insertion (PLI), the posterior scleral canal opening (PSCO), and the anterior end of the subarachnoid space (ASAS) (Fig. 1B). While marking in the sagittal section view window, the delineator simultaneously viewed a slaved window showing the cursor's location within a digital transverse section image (Fig. 1C). The 3-D Cartesian coordinates and category for each mark were saved, generating a 3-D point cloud that represented each of the marked structures (Fig. 1D).

Three experienced delineators performed all the delineations in this study. Both eyes of each animal were delineated by a single person. The delineators were not masked to the IOP status of each eye; however, they were effectively unaware of the IOP status during delineation, because the file name of each volume within the delineation software did not contain that information. On completion of delineation of both eyes of each monkey, the marks were checked for accuracy by two of the authors with extensive experience (HY, CFB) and without knowledge of IOP status.

The inter- and intradelineator variability and reproducibility of our delineation technique has been characterized in a series of reports.[24–26] Briefly, the interdelineator variability for each parameter was assessed by having five delineators (only two for our cupping parameters[25]) indicate all ONH landmark points within the normal and early-glaucoma eyes of three monkeys. Intradelineator reproducibility was assessed by having two of the five (only one for our cupping parameters) indicate all landmarks of both eyes of one monkey on two additional occasions at least 2 weeks apart. The inter- and intradelineator variability data from the three pairs of monkeys (one eye is normal and the contralateral eye is early-glaucoma) of our previous reports are summarized in Table 2.

Clinical Alignment of 3-D ONH Reconstructions

For each ONH, a reconstruction of the central retinal vessels was performed and three-dimensionally overlaid onto a predeath photo by using the qualitative match of the ONH and retinal vessels. Once preliminarily aligned (using the vessels only), the vessels and NCO points were co-visualized to assess the relationship of the optic disc margin in the photo to the delineated NCO points. A final 3-D adjustment was then performed to match the NCO to the disc margin while maintaining vessel alignment.

NCO Zero Reference Plane

For each 3-D ONH reconstruction, a least-squares ellipse was fit to the 80 NCO points (which in this case are the end of Bruch's membrane)[24,49] creating an NCO zero reference plane (Fig. 2C).[24] The centroid of the NCO ellipse established the center point for all measurements. All quantifications of offset, depth, position, and post-NCO total prelaminar volume were made relative to this plane (Figs. 2C–G).

Quantification

This report includes overall and regional quantification of neural canal offset and depth, lamina cribrosa position and thickness, scleral flange thickness, peripapillary scleral position and thickness, and post-NCO total prelaminar volume. The definitions and calculation methods of these parameters have been described in detail in our previous reports[24–26] and are briefly summarized as follows (Fig. 2). The neural canal landmark *depth* was the anterior-to-posterior distance of each marked point to the NCO zero reference plane, and *offset* was the distance (within NCO zero reference plane) of each projected mark

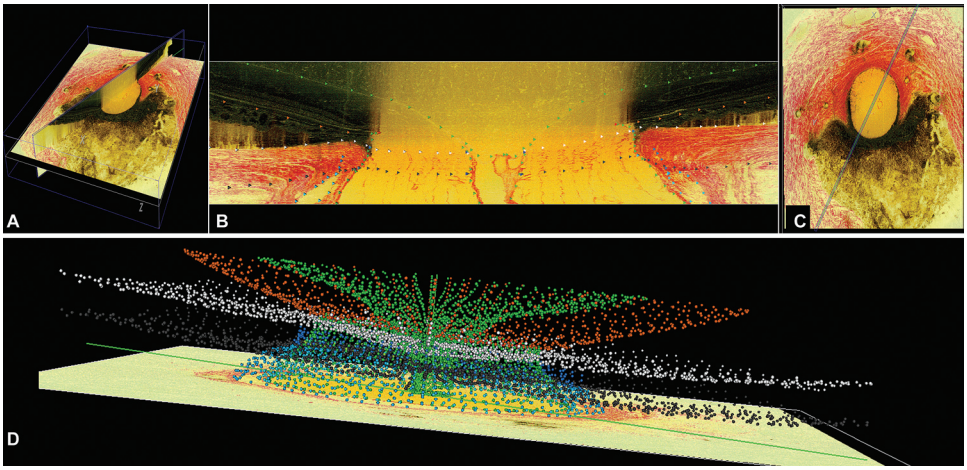

FIGURE 1. 3-D delineation within the colorized, stacked-section, 3-D ONH reconstruction of a single ONH. (**A**) Forty serial, digital, radial, sagittal slices, each 7 voxels thick, were served to the delineator at 4.5° intervals. (**B**) A representative digital sagittal slice, showing all 13 categories of the marks, which were 3-D delineated by using linked, simultaneous, colocalization of the sagittal slice (shown) and the transverse section image through the delineated point (**C**). (**D**) Representative 3-D point cloud showing all delineated points for a normal monkey ONH, relative to the posterior serial section image (vitreous, *top*; orbital optic nerve, *bottom*).

TABLE 2. Overall Parameters by Monkey

Parameters	Monkey 1		Monkey 2		Monkey 3		Monkey 4		Monkey 5		Monkey 6			Delineation Variability‡		
	Low IOP	H-L*	Low IOP	H-L	Low IOP	H-L	Low IOP	H-L	Low IOP	H-L	Low IOP	H-L	PID*max*†	Inter-D	Intra-D1	Intra-D2
Neural canal architecture (μm)																
NCO offset	509	1	586	19	663	16	501	−2	633	26	NA	NA	9	21	5	4
ASCO offset	644	−20	676	12	720	14	584	−2	657	9	562	58	16	10	10	12
ALI offset	645	−20	675	13	720	14	585	1	654	10	569	62	16	8	5	18
PLI offset	806	−21	797	31	828	13	702	−3	754	25	641	**100**§	18	18	17	6
PSCO offset	820	−15	825	23	877	−3	735	−5	801	11	658	**128**§	22	24	12	7
ASAS offset	951	−30	928	11	967	25	888	−16	875	28	781	**113**§	18	14	15	20
ASCO depth	21	7	54	−4	59	**−15**	55	−2	40	−7	61	−7	15	6	8	5
ALI depth	22	6	54	−4	61	**−16**	57	4	40	−5	70	−1	20	14	6	4
PLI depth	96	−5	146	**−28**§	142	**−11**	144	−7	147	**1**	210	**−55**§	20	13	19	2
PSCO depth	98	0	159	**−38**§	179	**−13**	158	−13	200	**−26**	224	**−47**§	27	23	12	1
ASAS depth	118	2	179	**−54**§	182	5	167	−25	207	**−22**	235	**−50**§	25	14	9	6
ONH connective tissue (μm)																
Lamina cribrosa position	−97	**−8**	−110	6	−131	**11**	−134	**−6**	−70	**−7**	−126	5	16	18	3	1
Lamina cribrosa thickness	90	**−2**	125	**−13**	133	**−13**	128	**−12**	129	**−11**	150	**−33**§	16	16	26	15
Peripapillary scleral position	2	1	−26	**22**§	−22	**12**	−28	**14**	−39	**22**§	−49	**17**	18	13	7	8
Peripapillary scleral thickness	115	**15**§	157	**−16**§	152	**11**	149	**−7**	173	**8**	196	**−39**§	14	38	5	10
Sclera flange thickness	58	0	77	−9	94	1	81	4	86	**12**§	NA	NA	5	14	12	11
ONH laminar cupping																
Post-NCO total prelaminar volume (mm^3)‖	0.126	7.7%	0.145	3.2%	0.223	−8.3%	0.145	10.6%	0.106	16.5%	0.122	18.0%	28.4%	11%	NA	2%

Bold: significant difference ($P < 0.05$) by ANOVA.

* Difference between high- and low-IOP eyes.

† PID*max* as previously reported.[28] Note that in most instances, the PID*max*, which represents the difference in the parameter between the two eyes in six bilaterally normal monkeys, exceeds the full range of the previously reported inter- and intradelineator variability.[24–28]

‡ Data were previously reported.[24–28] Interdelineator (Inter-D) variability is the range of variability in micrometers between five delineators, and intradelineator variability for two delineators (Intra-D1 and Intra-D2) is the range of variability in micrometers for each delineator on three delineation days.

‖ Statistical analysis is not applicable for this parameter. Percent differences between high- and low-IOP eyes for this parameter are reported.

§ Between-eye difference achieved statistical significance and exceeded the PID*max*.

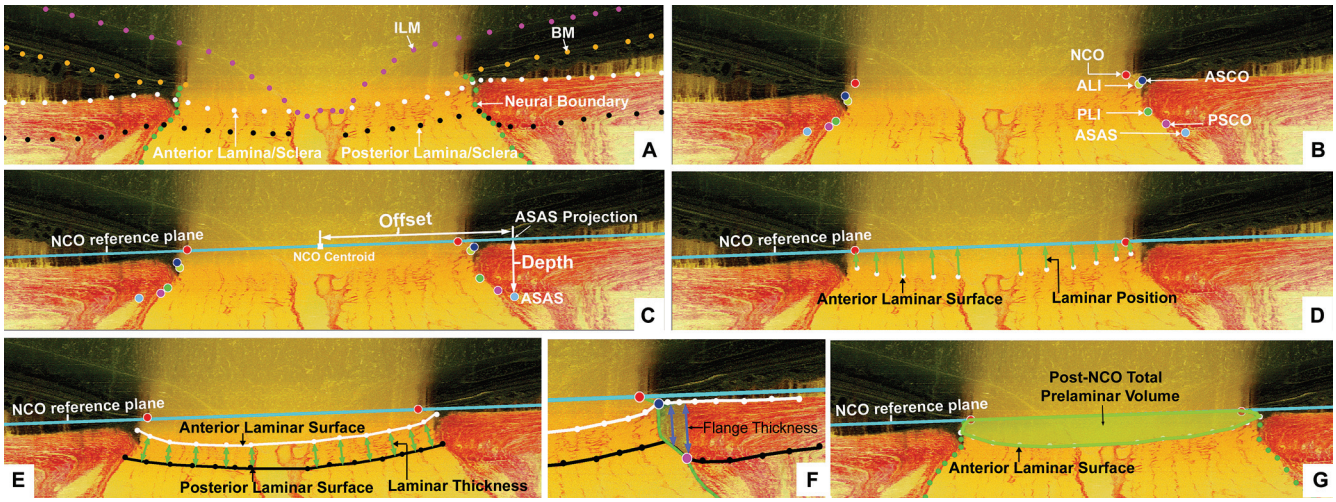

FIGURE 2. Parameter definitions: (**A**) a representative digital sagittal slice showing the ILM (*pink dots*), BM (*orange dots*), anterior laminar/scleral surface (*white dots*), posterior laminar/scleral surface (*black dots*), and neural boundary (*green dots*). (**B**) A representative digital sagittal slice showing the neural canal architecture: NCO (the opening in the Bruch's membrane/retinal pigment epithelial complex, *red*), ASCO (*dark blue*), ALI (*dark yellow*, partly hidden behind the ASCO in *dark blue*), the PLI (*green*), and PSCO (*pink*).The ASAS (*light blue*) was also delineated. (**C**) Definitions of the offset and depth using ASAS as an example. *Right* ASAS point was projected to NCO zero reference plane (*cyan line*), the distance between NCO centroid to the projection of ASAS was defined as *offset*. The distance between the ASAS to the projection was defined as the *depth* of ASAS. The offset and depth of all other neural canal structures were defined in the same way. (**D**) *Laminar position* (*green arrow*) is defined as the shortest distance from the delineated anterior laminar surface point (*white dot*) to the NCO zero reference plane. (**E**) *Lamina cribrosa thickness* at each delineated anterior surface point is determined by fitting a continuous surface (*white line*) to all anterior surface points and then measuring the distance along a normal vector of the anterior surface (*green arrow*) from each anterior delineated point to the posterior surface. (**F**) The thickness of the scleral flange at each delineated anterior surface point (*white dots*) is defined as the distance between the neural canal boundary points (*green line*), along a vector parallel to the PSCO normal vector (*blue arrow*). (**I**) *Post-NCO total prelaminar volume* (*light green*: a measure of the laminar or connective tissue component of cupping) is the volume beneath the NCO zero reference plane in *cyan*, above the lamina cribrosa and within the neural canal wall.

from NCO centroid. *Laminar position* was the shortest distance from each delineated anterior laminar surface point to the NCO reference plane. *Laminar thickness* was calculated at each delineated anterior laminar surface point as the shortest distance to the posterior laminar surface along a vector normal to the anterior laminar surface (fitted into the continuous surface to generate the normal vector).

Peripapillary scleral position and thickness were calculated in the same way as laminar position and thickness. *Scleral flange thickness* was defined as the distance from the anterior scleral flange surface to the neural canal boundary surface, measured at each delineated anterior scleral flange surface point along a vector parallel to the PSCO normal vector. *Post-NCO total prelaminar volume* was designed to detect deformation of the anterior neural canal connective tissue in a single parameter and is defined to be the total volume (tissue and nontissue) beneath the NCO zero reference plane, above the lamina cribrosa, and within the neural canal wall.

Overall and Regional Intereye Differences by Monkey

Overall and regional parameter values were calculated for both eyes of each monkey as outlined in Figure 3.

Overall and Regional Schematic Data Maps by Monkey

Schematic depictions of overall (Fig. 4) and regional (Fig. 5) differences were created without regard for statistical significance for each monkey by overlaying the overall mean measurements for each eye (Fig. 4) or for the superior and inferior (Fig. 5, left) and nasal temporal (Fig. 5, right) regions of each eye.

Statistical Analyses

For each ONH, 80 measurements of the following parameters were made: offset and depth of the ASCO, ALI, PLI, PSCO, and ASAS. Measurement of laminar position and thickness, scleral flange thickness, and peripapillary scleral position and thickness were made at each delineation point after the surfaces were fit to the anterior and posterior laminar and scleral points. Therefore, for all nonvolumetric parameters, at least $n = 40$ measurements were made for each ONH, and a factorial analysis of variance (ANOVA) was performed to assess the effect of region and IOP (IOP-10 vs. IOP-30 or IOP-10 vs. IOP-45) on each parameter between the eyes of each monkey. Statistically significant differences between regions, IOPs, and region-by-IOP combinations required an overall significant *F*-test followed by *t*-tests with *P* corrected for multiple comparisons.[50] Because our volumetric parameters did not lend themselves to multiple measures within individual eyes, a statistical assessment of intraeye differences for post-NCO total prelaminar volume for each monkey was not possible.

Statistically Significant and EPID*max* Differences

As just described, statistically significant differences were determined by an ANOVA. We defined EPID*max* differences to be those statistically significant differences that exceeded the physiologic intereye difference maximum (the maximum intereye difference; PID*max*) within six bilaterally normal monkeys in a previous report.[28] Within this construct, we considered statistically significant differences between the high- and low-IOP eyes of each monkey to be those that exceeded the combination of the variability of our 3-D histomorphometric quantification method and the true biological variation of each parameter both overall and within a region. We considered EPID*max* differences to be those statistically significant differences that were more likely to be treatment effects (i.e., to represent a biological response to acute pressure elevation rather than the difference between the eyes of a normal monkey). For each volumetric parameter, we compared the intereye difference for each animal to the PID*max* difference for that parameter and

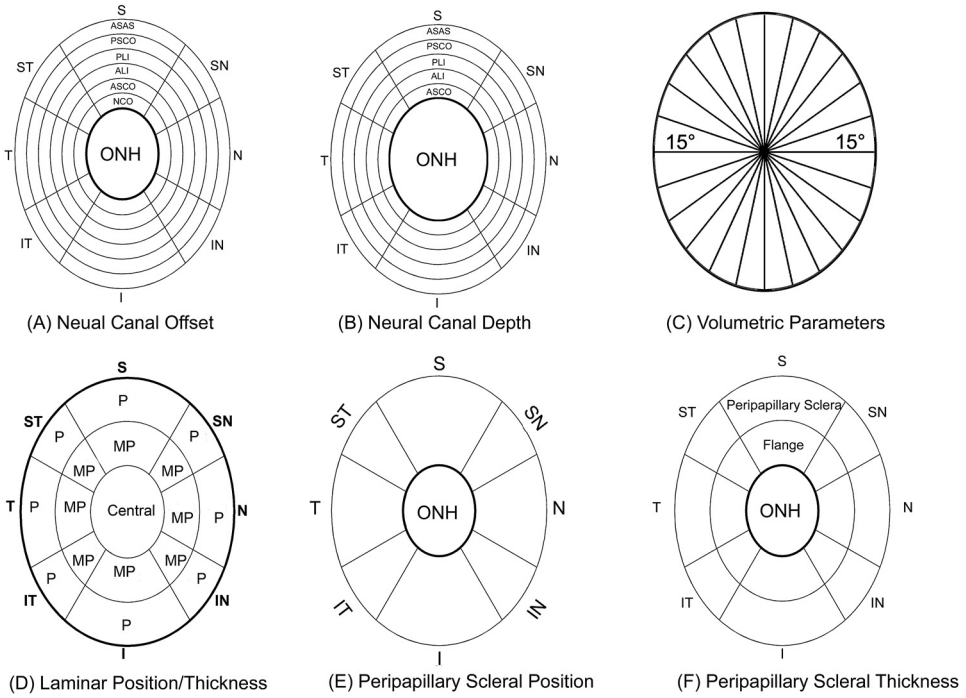

FIGURE 3. Parameter regionalization (right eye configuration)**.** Neural canal offset (**A**) and depth data (**B**) for each neural canal landmark were pooled for eight anatomic regions: superior (S), superonasal (SN), nasal (N), inferonasal (IN), inferior (I), inferotemporal (IT), temporal (T), and superotemporal (ST). The S, N, I, and T regions contained all marks within 60° sections of the ONH centered about the S-I and N-T clinical axes, and the SN, IN, IT, and ST regions contained all marks in 30° radial sections of the ONH centered about the SN-IT and IN-ST axes. Concentric rings represent the different neural canal landmarks from its internal entrance NCO to its external exit PSCO as shown in the superior region of (**A**) and (**B**). Neural canal depth measurements started with the ASCO rather than NCO. (**C**) With the center of the NCO as the starting point, 12 radial sections perpendicular to the NCO zero reference plane divided the volumetric parameters into 24, 15° radial regions. Then, regional volumes were projected onto the NCO zero reference plane, color-coded by region and overlaid onto a standard ellipse. (**D**) Within the lamina, position and thickness data were pooled into 17 regions according to the three radial regions (central; MP, middle periphery; P, periphery) and eight quadrants, as in (**A**) and (**B**). (**E**) The peripapillary sclera position data were pooled into eight regions (inner boundary starting from the ASCO ellipse [*dark black line*] to an ellipse that is 1.62 times the size of the ASCO ellipse). (**F**) Peripapillary scleral thickness data were pooled into 16 regions; 2 radial regions (flange, covering the area from ASCO to PSCO; peripapillary sclera region, covering the area from PSCO to 1.62 times ASCO size).

defined EPID*max* differences to be those differences that exceeded the PID*max* only.

Difference, Change, and Deformation Terminology

We measured postmortem intereye differences for each parameter for each monkey. We emphasized EPID*max* intereye differences as those statistically significant differences that most likely represent acute IOP-induced change in the high-IOP eye of each monkey. We thus referred to EPID*max* intereye differences as *change* or *EPIDmax change*.

We further grouped our parameters into *position-change* and *thickness-change* parameters to better recognize the colocalized behavior of these two forms of deformation. To describe *position-change* we used the following terminology as it relates to EPID*max* differences in our measurement parameters: *neural canal radial expansion* was defined to be an EPID*max* increase, *neural canal radial contraction* an EPID*max* decrease in neural canal offset, *lamina cribrosa anterior deformation* was defined to be an EPID*max* increase (more anterior or inward), and *lamina cribrosa posterior deformation* an EPID*max* decrease (more posterior or outward) in anterior lamina cribrosa position, relative to the NCO zero reference plane.

Peripapillary scleral posterior bowing was defined to be a posterior (outward) deformation of the peripapillary sclera relative to the more peripheral sclera, which manifests as an EPID*max* increase in the position of the peripapillary sclera. In this scenario, because the peripapillary sclera carries the ONH with it as it moves outward, it assumes a final position that is anterior to the NCO zero reference plane. *Post-NCO total prelaminar volume expansion* was defined as an EPID*max* volumetric increase and *post-NCO total prelaminar volume contraction* an EPID*max* volumetric decrease in the space confined below the NCO zero reference plane, within the neural canal wall and above the anterior laminar surface. As such, this parameter volumetrically combines the individual deformations of the neural canal wall and lamina cribrosa relative to the NCO zero reference plane.

To describe *thickness-change*, we defined *neural canal axial thickening* to be an EPID*max* increase, and *neural canal axial thinning* an EPID*max* decrease in neural canal landmark depth. We defined *laminar* and *peripapillary scleral thickening and thinning* as EPID*max* increases or decreases in the thickness measurements for each tissue.

RESULTS

Descriptive Data

Descriptive data for the six normal monkeys and the histomorphometric optic disc size for each eye are reported in Table 1. Five rhesus monkeys and one cynomolgus monkey, aged from 5 to 14 years, were used. Mean IOP under ketamine/xylazine anesthesia varied from 4 to 12 mm Hg in both eyes of all six monkeys. Ultrasonic axial length measurements before death ranged from 18.29 to 21.39 mm.

Histomorphometric vertical disc size (measured at NCO) ranged from 1214 to 1641 μm, and histomorphometric horizontal disc size ranged from 864 to 1143 μm. Histomorphometric optic disc area ranged from 0.801 to 1.473 mm^2 (based on an ellipse fitted to 80 delineated NCO points; see the Methods section).

Overall Data for Each Parameter by Monkey

Overall IOP-10 eye data along with the statistically significant and EPID*max* differences for the high-IOP eye of each animal are reported in Table 2. Schematic plots of the overall data for both eyes of each monkey are presented in Figure 4.

Within the schematic plots of Figure 4, qualitative differences between the 6 low-IOP normal eyes include laminar surface curvature (relatively flat in monkey 5 and relatively curved in monkeys 1 and 4); laminar and peripapillary thickness (relatively thin in monkey 1 and relatively thick in monkey

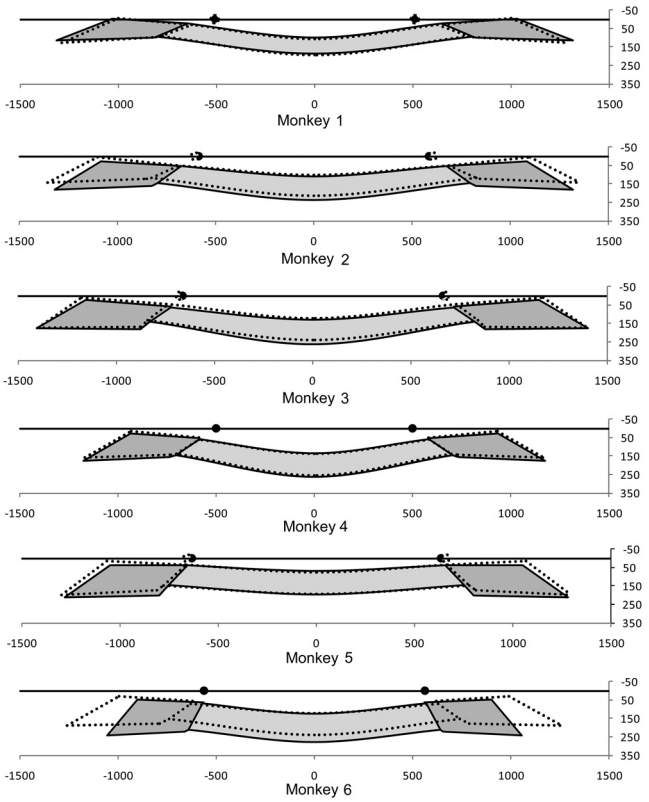

FIGURE 4. Schematic representation of the overall deformation data for the low (*solid colors*)- and high (*dotted lines*)-IOP ONHs of each monkey as reported in Table 2. Qualitative differences between the six normal eyes include laminar surface curvature (relatively flat monkey 5, relatively curved monkeys 1, 4); laminar and peripapillary thickness (relatively thin monkey 1, relatively thick monkey 6); and NCO size and obliqueness (small and less oblique monkey 6, large and more oblique monkey 3). Intereye differences after acute IOP elevation were greatest in monkeys 5 and 6 and include radial expansion of the scleral portion of the neural canal posteriorly, accompanied by axial thinning of the posterior canal, thinning of the lamina without substantial posterior deformation, and posterior bowing of the peripapillary sclera. These changes were minimally and variably present in the other four eyes. There was no qualitative relationship between the geometry, magnitude of IOP, and degree of deformation in the high-IOP eyes.

6); and NCO size and obliqueness (small and less oblique in monkey 6, and large and more oblique monkey 3). Overall, the lamina cribrosa did not deform appreciably in the high-IOP eyes of any of these monkeys compared to their contralateral IOP-10 eye. Intereye differences after acute IOP elevation are greatest in monkeys 5 and 6 and include expansion and thinning of the posterior neural canal, accompanied by thinning of the lamina without substantial posterior deformation of the lamina cribrosa and posterior bowing of the peripapillary sclera.

Within the overall data in Table 2, very few changes achieved EPID*max* differences and therefore we emphasize the regional rather than the overall results.

Regional Data for each Parameter by Monkey

Superimposed, averaged, central vertical, and horizontal data for both eyes of each animal are schematically depicted in Figure 5. Statistically significant and EPID*max* regional differences for each parameter and for each monkey are reported in Figure 6. Although the overall deformations depicted in Figure 4 were minimal, the schematics (Fig. 5) qualitatively established that regional alterations were more substantial. When the regional intereye difference data for each position and thickness parameter were arranged by monkey (Fig. 6), three patterns of change were apparent. Monkey 1 demonstrated minimal regional position or thickness change. Monkeys 2, 3, and 4 demonstrated non-colocalized regional thinning and peripapillary scleral bowing. Monkeys 5 and 6 demonstrated colocalized regional thinning and position changes. These three patterns of early IOP-induced alterations and the fact that each included minimal laminar position change, are the principal findings of this report.

Minimal Detectable Change

Although the high-IOP eye of monkey 1 demonstrated overall peripapillary scleral thickening (Table 2) and a region of colocalized neural canal thinning and peripapillary scleral posterior bowing and thickening (Fig. 6), these changes were of minimal magnitude and extent.

Non-colocalized Regional Thinning, Canal Expansion, and Peripapillary Scleral Bowing

Monkeys 2, 3, and 4 demonstrated EPID*max* thinning of the neural canal and lamina and non-colocalized peripapillary scleral bowing.

Colocalized Regional Thinning and Position Changes

Monkeys 5 and 6 demonstrated enough regional position and thickness change that these phenomena colocalized. The phenomenon of colocalization was not precise, but was best seen in the regions of EPID*max* post-NCO total prelaminar volume expansion, which broadly colocalized with regional neural canal expansion and thinning as well as peripapillary scleral bowing in each eye.

Effect of Magnitude and Duration of IOP Elevation

There was no evidence of increased deformation in the IOP-45 (monkeys 1–3) compared to the IOP-30 (monkeys 4–6) eyes after 15 minutes of acute IOP elevation, either overall or regionally. However, the most extensive deformation clearly occurred within the one animal (monkey 6) in which the acute IOP elevation to 30 mm Hg was held for 30 rather than 15 minutes.

Discussion

The purpose of this study was to three-dimensionally quantify the laminar, neural canal wall, and peripapillary scleral components of ONH connective tissue deformation after 15 minutes of acute IOP elevation in five monkeys (30 minutes in monkey 6). The principal findings of this report are as follows. First, in all animals, the lamina deformed minimally in the high-IOP eye and was not only posterior but in some cases anterior. Second, all deformations (both position and thickness changes) were regional and specific to individual eyes. Third, the regional deformation within the six high-IOP eyes spanned the following spectrum: minimal detectable change in monkey 1; regional thinning accompanied by non-colocalized peripapillary scleral bowing in monkeys 2, 3, and 4; and colocalized regional thickness and position changes in monkeys 5 (superior temporally and temporally) and 6 (inferior temporally and temporally). Fourth, by far the greatest deformation occurred in the one eye subjected to 30 minutes of elevated IOP. Fifth, neither the magnitude of IOP elevation nor the architecture of the ONH connective tissue appeared to relate to the magnitude of deformation.

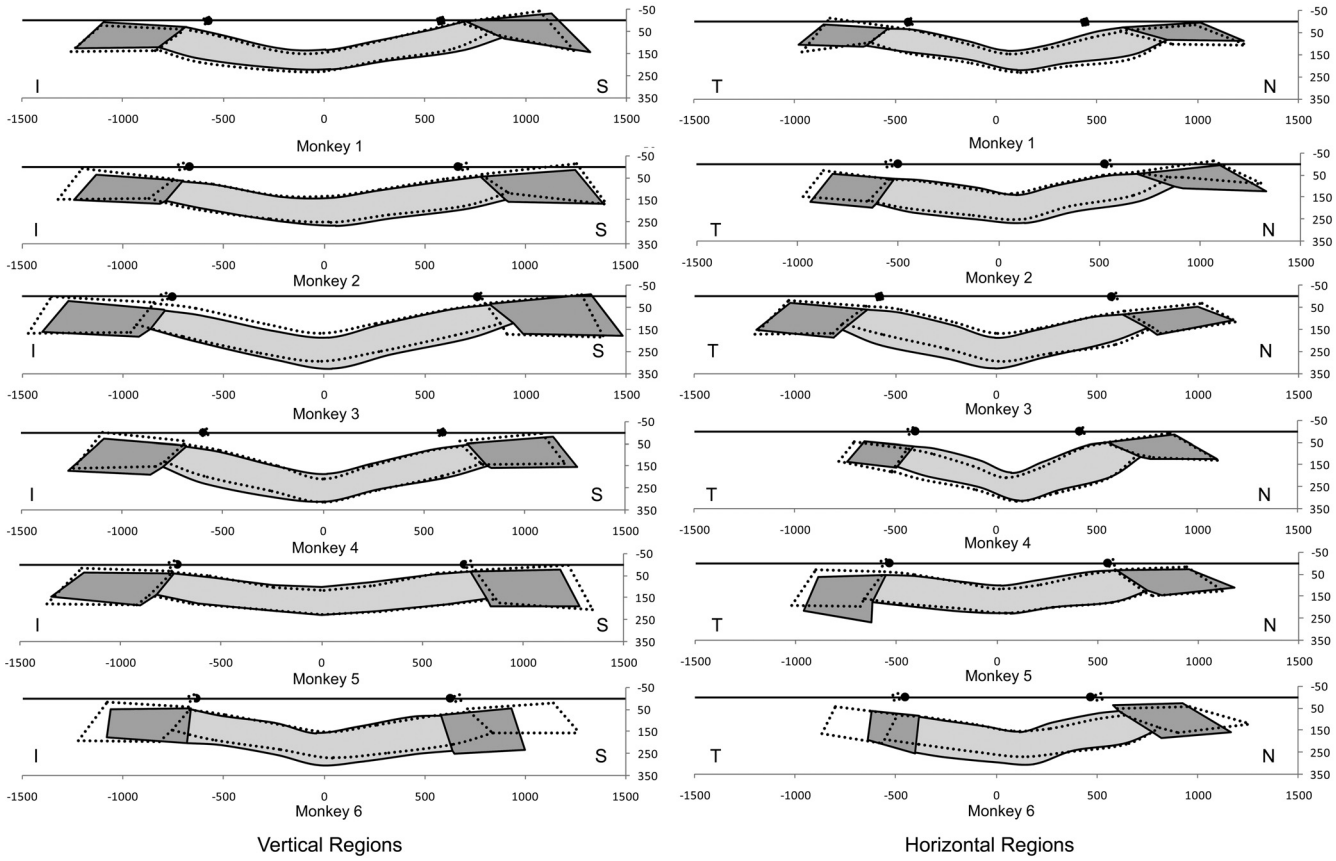

FIGURE 5. Schematic representation of the vertical and horizontal regional deformation data for the low (*solid colors*)- and high (*dotted lines*)-IOP ONHs of each monkey. Mean data from the superior and inferior (*left*) and nasal and temporal (*right*). Regions of both eyes of each animal are schematically overlaid as central vertical (*left*) and horizontal (*right*) sections. The net regional canal expansion can now be seen in monkeys 2, 3, 5, and 6 (although in monkey 1, there was contraction of the superior canal). Small overall posterior bowing of the peripapillary sclera was present in most animals. Small anterior and posterior deformations of the lamina cribrosa accompanied by laminar thinning were also present in most high-IOP eyes. The canal, laminar, and peripapillary sclera deformations were not symmetrical to the center of the NCO in some animals because of the true asymmetric deformation and asymmetric neural canal architecture within the two eyes of an animal. Although the recorded intereye differences are accurate, they are a likely combination of true connective tissue deformation plus some reference-plane–induced artifacts in the subset of high-IOP eyes, in which true connective tissue deformation led to shifts and/or tilts in the position of the reference plane relative to the structures being measured. All data are plotted in right eye configuration.

These findings should be viewed in the following context. First, the lack of substantial laminar deformation in these animals is compatible with our previous study[19]; with that of Levy and Crapps,[22] in which the period of IOP elevation was short; and with recent studies in which spectral domain optical coherence tomography (SD-OCT) was used in living human eyes (Agoumi Y, et al. *IOVS* 2009;49:ARVO E-Abstract 4898). These findings are also consistent with predictions made by computational models devised by Sigal et al.[51] Using eye-specific models, they observed that an acute increase in IOP led to peripapillary sclera bowing and lateral displacements of the lamina (mostly in the periphery), whereas the central lamina remained stationary or displaced slightly anteriorly, depending on the eye. The study, however, did not address the differences in ONH architecture that led to the variations in response to IOP.

Our deformations were less than those reported by Yan et al.[21] in which IOP was increased for 24 hours. Laminar and scleral canal wall deformations are likely to be viscoelastic,[23,52] meaning that the tissue reaches full deformation only after a given period, and so longer IOP elevations may induce larger deformations. Although ex vivo studies of human eyes suggest that an equilibration time of 15 minutes is sufficient to obtain a stable deformation of the vitreoretinal interface,[53] it is possible that the deformations in this study would have been more substantial had the period of IOP elevation been extended to hours or days. Based on our previous studies of connective tissue architecture in monkey eyes[19,48] and recent parameterized finite element modeling of human[51,54–56] and monkey (Sigal IA, et al. *IOVS* 2008;49:ARVO E-Abstract 3668; Roberts MD, et al. *IOVS* 2008;49:ARVO E-Abstract 3669) ONHs, we believe that the manner in which the lamina cribrosa and/or scleral canal deform after a given IOP elevation is determined by the level and duration of IOP elevation and the structural stiffness of each tissue.

The structural stiffness of a tissue is the combination of its architecture (the quantity and distribution of load-bearing tissue) and its material properties (the stiffness or compliance of the tissue), both of which contribute to a structure's ability to withstand deformation under an applied load.[57] The results obtained in this work suggest that the structural stiffness of the lamina cribrosa and peripapillary sclera interact (Fig. 7), which is consistent with our previous report[48] and predictions made with computational models.[57,58] For analysis, it is useful to separate the IOP-induced deformation of the ONH tissues into scleral canal expansion or contraction, laminar and scleral canal thinning, and anterior or posterior laminar and peripapillary sclera deformation. Within this lamina–sclera dynamic,

the structural stiffness of the peripapillary sclera largely governs whether the scleral canal expands after an increase in IOP. When the structural stiffness of the sclera is relatively low, an increase in IOP produces an expansion of the canal, pulling on the lamina—an indirect effect of IOP on the lamina itself. When, instead, the structural stiffness of the sclera is relatively high, an increase in IOP produces a much more modest expansion of the canal. In this case the lamina cribrosa is not pulled taut and is left to resist the direct force of IOP with its structural stiffness alone, deforming posteriorly. We believe that, in most eyes, the situation would not be at either of the extremes described, but rather some combination of the two cases. It should be noted that even in the setting of minimal anterior or posterior laminar deformation, substantial tensile strain (local deformation) within the laminar beams may be induced by the expanding scleral canal.[51]

Second, the fact that all deformations (both position and thickness changes) were regional and specific to each eye is best appreciated within the regional data of Figure 6. In saying that the deformations were regional, we mean that the EPID*max* deformations were focal (only one region) or regional (at least two regions), or they were greatest within a single region when diffuse (monkey 6 only). By individual-eye–specific, we mean that the regions of greatest deformation were not consistent within these six high-IOP eyes. We believe our study is the first to establish that early ONH connective tissue deformation after acute IOP elevation is regional and is likely to be individual-eye–specific.

Third, we observed three patterns of acute ONH connective tissue deformation within these six animals: minimal deformation; non-colocalized regional thinning and peripapillary scleral bowing; and colocalized position and thickness changes. To determine whether the observed deformations are portions of a continuum of ONH connective tissue deformation necessitates the development of SD-OCT[49,59,60] (Agoumi Y, et al. *IOVS* 2009;49:ARVO E-Abstract 4898) or second-harmonic imaging[61] to capture these same ONH landmarks at multiple time points after acute IOP elevation in living human and monkey eyes. Regardless of whether these patterns are part of a continuous spectrum of connective tissue deformation, our data strongly suggest that laminar and neural canal thinning, neural canal expansion, and peripapillary sclera bowing are early responses to acute IOP elevation in the monkey eye and that, within the limits of our experimental techniques, these phenomena colocalize within those eyes demonstrating the greatest deformation.

Fourth, by far the greatest deformation occurred in the one eye subjected to 30 minutes of elevated IOP even though pressure was only raised to 30 mm Hg. This animal, which was among the younger animals, but not the youngest, had the thickest lamina and peripapillary sclera and the smallest scleral canal (Table 2, Figs. 4, 5). It could be that the duration of IOP exposure is an important determinant of acute ONH connective tissue deformation. Several investigators have reported substantially increased ONH connective tissue deformations after the prolonged application of load.[21,62,63] It is possible that the additional duration of IOP elevation and time-dependent (or viscoelastic) effects alone, account for the magnitude of deformation in monkey 6. However, without more eyes exposed to longer IOP elevations and/or a series of individual eyes imaged at multiple time points after acute IOP elevation, the data from this one animal did not support such a viscoelastic effect.

It is also possible that monkey 6 simply had a much more compliant lamina and sclera than did the other animals. In our previous histologic study of ONH connective tissue compliance,[19] none of the normal monkeys achieved this magnitude of deformation, although some experienced up to 80 minutes of IOP elevation. This, along with the fact that this animal appeared to have the thickest lamina and sclera and smallest scleral canal (Table 2, Figs. 4, 5), suggests that the material properties of both the lamina and sclera in this eye were substantially less stiff than were the other five high-IOP eyes. Estimates of these material properties within engineering finite element models[64,65] will be the subject of a future report.

Fifth, neither the magnitude of IOP elevation nor the tissue-level architecture of the ONH connective tissue closely correlates to the magnitude of connective tissue deformation. Although we believe that there should be consistent biomechanical determinants of ONH connective tissue behavior, these relationships are not obvious from the histomorphometric measurements in this report. Elucidating these relationships is one of the goals of ongoing finite element modeling.[54,58,64]

Our findings are limited by the following considerations. Although we recently improved our 3-D histomorphometric methodologies to acquire data by using $1.5 \times 1.5 \times 1.5$-$\mu$m voxels,[28] all the reconstructions in this study were acquired with our older $2.5 \times 2.5 \times 3.0$-$\mu$m voxel technique. Most of the differences we report substantially exceed the resolution of these 3-D reconstructions, and we have previously demonstrated good reproducibility of our delineation techniques at this resolution.[24–26] In addition, there were tissue shrinkage effects from both fixation and embedding associated with this technique, but comparisons between the two eyes of each monkey should be valid, since all eyes were treated identically.

For this study, we chose acute IOP elevations of 15-minute duration for two reasons. First, our previous ONH surface compliance testing had suggested that most ONH surface deformation during 60 minutes of acute IOP elevation occurred during the first 15 minutes of elevated IOP.[66,67] Second, perfusion fixation is performed under deep pentobarbital anesthesia, which can lower systemic blood pressure (BP). In other animals, we had seen evidence of poor perfusion of the central retinal vessels in eyes that were perfusion fixed after 30 to 80 minutes of high IOP. However, even in the five high-IOP eyes of this report using our old euthanasia protocol, blood pressures were low at the time of perfusion, and we saw evidence of residual blood within the retinal and posterior ciliary circulation that suggested less than ideal fixative perfusion. This residual blood may also have been present because the fixative perfusion pressure was not high enough (3–4 psi) to push the fixative fluid into the small arteries of the ONH, due to the flow-limiting nature of the old perfusion system.

Although all eyes maintained their set IOP for 60 minutes after perfusion, it is possible that our data underestimated the magnitude of acute IOP-induced deformation of ONH connective tissue if fixation was less than ideal. However, our most current protocol, which ensures a fixative perfusion pressure of 80 mm Hg as measured by direct real-time pressure monitoring via brachial artery cannulation, was used in the euthanasia of monkey 1. We did not see larger connective tissue deformations in this monkey, which suggests that the small deformations we report for the other monkeys are not artifactual.

Our study may also underestimate the laminar component of ONH connective tissue deformation after acute IOP elevation if cerebrospinal fluid (CSF) pressure became elevated during the period of perfusion, and retrolaminar tissue pressure was inadvertently elevated as a result.[68] We did not monitor the CSF pressure in these experiments; however, we think that this phenomenon is unlikely for the following reasons. First, as outlined earlier, BP during perfusion was probably low in the first five eyes and was not greater than 80 mm Hg in the sixth. Although the relationship between BP change and CSF pressure change in an animal that is undergoing fixation with glutaraldehyde has not been characterized, the fact that BP was

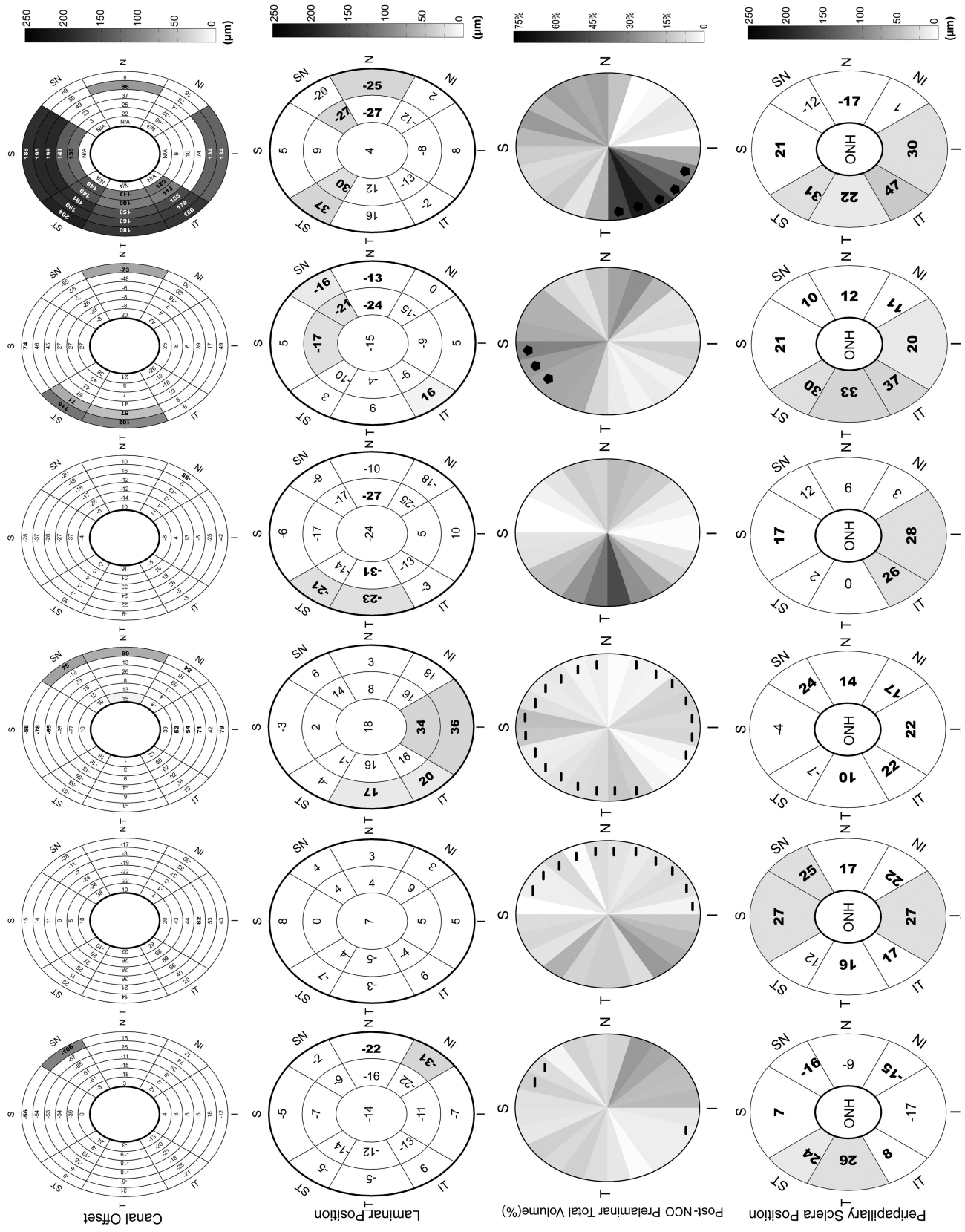
Monkey 1
Monkey 2
Monkey 3
Monkey 4
Monkey 5
Monkey 6
Peripapillary Sclera Position
Post-NCO Prelaminar Total Volume(%)
Laminar Position
Canal Offset
ONH
(μm)
250
200
150
100
50
0
75%
60%
45%
30%
15%
S
I
T
N
NI
NS
SN
SI
ST
IT
IN

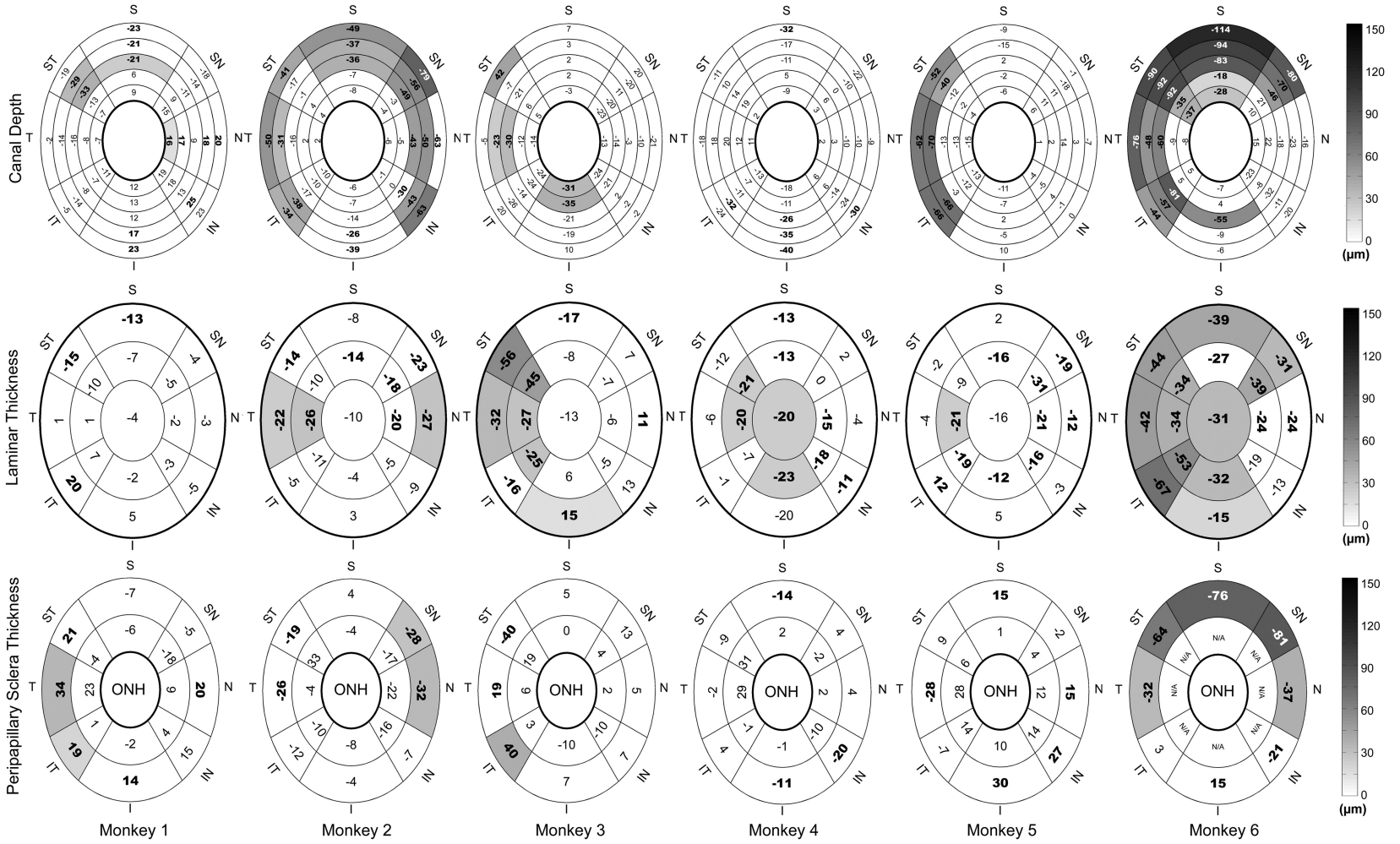

Figure 6. Regional parameter difference maps for the high-IOP eyes by monkey (*columns*) and by parameter (*rows*). These maps demonstrate the regional colocalization of statistically significant (*bold*, $P < 0.05$, ANOVA) and EPID*max* (*shaded*)[28] differences within the high-IOP eye of each animal. Data are the magnitude of change in the high-IOP eye relative to its contralateral low IOP control. Positive and negative data in the colored regions are defined for each parameter as follows: canal offset—radial expansion/radial contraction of the canal; lamina cribrosa position—anterior (inward) movement/posterior (outward) of the anterior laminar surface; post-NCO total prelaminar volume—expansion/contraction of the space beneath the NCO zero reference plane, above the lamina and within the neural canal wall. For post-BMO total prelaminar volume, regional differences that exceeded PID*max* differences are marked by stars and regions with negative volume change (contractions) are marked with a negative sign. Positive peripapillary scleral position—anterior (inward) shift of the peripapillary sclera relative to the NCO zero reference plane, which most likely reflects posterior (outward) bowing of the peripapillary sclera and NCO zero reference plane (together) relative to the more peripheral sclera; canal depth—axial thickening/axial thinning of the canal; lamina cribrosa thickness—thickening/thinning; peripapillary scleral thickness—thickening/thinning of the peripapillary sclera. All data are plotted in right-eye configuration. S, superior; SN, superonasal; N, nasal; IN, inferonasal; I, inferior; IT, inferotemporal; T, temporal; ST, superotemporal. See Figure 3 for a detailed description of regionalization.

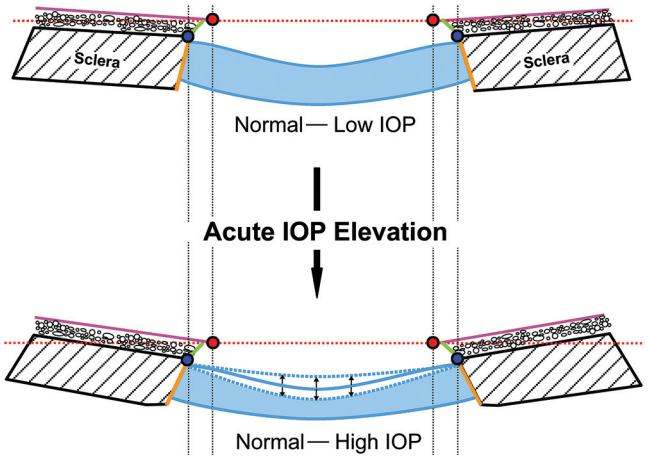

FIGURE 7. A peripapillary scleral–lamina cribrosa dynamic underlies ONH biomechanics.[48] We propose that there are peripapillary scleral and lamina cribrosa contributions to ONH connective tissue behavior and that the manner in which the scleral canal and lamina cribrosa deform after a given level of IOP elevation in a given ONH will be determined by its level and duration and the structural stiffness of each tissue. *Top*: normal lamina cribrosa (*light blue*), peripapillary sclera (*slanted lines*), Bruch's membrane (*solid pink line*), NCO (*red circles*: in this schematic diagram, Bruch's membrane extends into the canal and is thus considered the NCO); anterior scleral opening (*blue circles*); NCO zero reference plane (*dotted red line*); border tissue of Elschnig (*light green*); choroid (*black circles*); and the scleral portion of the neural canal (*orange*). The structural stiffness of a tissue is defined as the combined function of both its connective tissue architecture (the quantity and distribution of load-bearing tissue) and material properties (the stiffness or compliance of the tissue). *Bottom*: changes after acute IOP elevation in the monkey eye, as depicted in this diagram, can include: (1) posterior bowing of the ONH and circumpapillary sclera relative to the more peripheral peripapillary sclera (which manifest as an anterior deformation of the peripapillary sclera relative to the NCO zero reference plane); (2) axial thinning (*orange lines* are smaller in the high-IOP eye) and radial expansion of the posterior scleral portion of the neural canal; (3) laminar thinning (*solid blue* at high IOP is less than low IOP); and (4) small anterior or posterior deformations of the anterior lamina cribrosa surface (*black arrows* and *dotted blue lines*). The effects of these deformations on astrocyte physiology, posterior ciliary artery blood flow, and retinal ganglion cell axon axoplasmic transport and flow remain to be determined.

low in most eyes suggests that CSF pressure was also low. Second, we qualitatively compared the size of the anteriormost portion of the subarachnoid space within the 3-D histomorphometric reconstructions of the other five monkeys (perfusion fixed at low BP) to monkey 1 and found no obvious difference. This suggested that the volume of the CSF space was not altered by the higher perfusion BP in monkey 1. Finally, even if CSF pressure slowly climbed during the period of perfusion fixation, this process would have occurred at the same time that the connective tissues were being fixed into a position determined by the previous 15 minutes of IOP elevation. We doubt that a slow CSF increase would alter the effects of glutaraldehyde being delivered to the tissues via the blood vessels.

However, a qualitative inspection of the subarachnoid space in all our perfusion- and immersion-fixed tissues[19,20,24–26,28] suggests that the subarachnoid space is expanded in the perfusion-fixed eyes. Although the collapsed (immersion-fixed) versus expanded (perfusion-fixed) subarachnoid space may only represent the effects of physiologic CSF pressure (in the perfusion-fixed eyes), elevated CSF pressure in the animals in this study affecting the laminar (but not the scleral) deformations remains a possibility and may necessitate further investigation.

It is possible that trephining a 6-mm-diameter piece of the ONH and peripapillary sclera allowed residual stresses within the sclera to be relieved. The resultant postfixation tissue warping, if present, could induce non–IOP-related alterations in tissue position that would confound our measurements. However, these effects would most likely occur in the peripheral sclera closest to the trephine edge and therefore are unlikely to affect the measurements within the ONH and peripapillary sclera. In addition, we believe that a large degree of tissue warping in the setting of months of glutaraldehyde fixation is unlikely.

All our measurements were made relative to a plane based on the delineated NCO points (which are the end of Bruch's membrane in most monkeys).[24] Any collapse of the border tissue of Elschnig or compression of the choroid either from the period of high IOP or from posttrephination tissue warping, could have altered these points, leading to a posterior shift or tilt of the reference plane in the high-IOP eye, which would have induced anterior movement or tilting of the other structures relative to its contralateral normal. In the case of reference plane tilt, the effect would be greatest in the periphery and least near the point of inflection. In the case of a posterior shift, the effect would be similar in both central and peripheral measurements.

We believe that the measurements we report for both eyes of each animal are accurate based on the previously reported reproducibility of our delineation method and the voxel dimensions within our reconstructions.[24–26] We do not believe that important shifts in the reference plane occurred as a result of focal alterations in the border tissue of Elschnig architecture or choroidal compression within the high-IOP eyes for the following reasons. First, overall thinning of the ASCO and ALI achieved statistical (but not EPID*max*) significance in monkey 3 only. Regional EPID*max* thinning of the anterior neural canal was present only in monkey 3 and 6. A small tilting effect was also seen within the regional cross-section schematics for monkeys 3 and 6 (Fig. 5), wherein the high-IOP ONH seemed to be slightly rotated relative to the low-IOP ONH.

The lack of substantial anterior scleral canal thinning in all six animals is important because it suggests that little posterior deformation of NCO relative to the ONH and peripapillary scleral landmarks that we studied (as might happen if the choroid was compressed, or the border tissue of Elschnig was deformed by the acute IOP elevations) is present in any of the six high-IOP eyes. The fact that the regional EPID*max* posterior canal thinning detected in monkeys 1, 2, 5, and 6 greatly exceed the anterior canal thinning within their same regions (significant or otherwise) strongly suggests that the detected posterior canal thinning in these animals was not a measurement artifact.

Second, we closely examined the 0°, 30°, 60°, 90°, 120°, and 150° digital section images from both eyes of each animal and found no qualitative evidence of choroidal compression in the high-IOP eyes. In fact, in all monkeys the choroid was substantially expanded, even in the face of the elevated IOP in the high-IOP eye.

Our study included five rhesus and one cynomolgus monkey, which may confound our results. Although there may be species differences in normal monkey ONH connective tissue architecture and material properties that could influence their response to acute IOP elevation,[19,20,69] we doubt that these are important in our study for the following reasons. First, by qualitative comparison the normal eye measurements of monkey 4 (cynomolgus) fell within the range determined by the five rhesus animals for each parameter, except for NCO offset and laminar position, where they were only minimally out of

that range (Table 2). Second, the overall behavior in the high-IOP eye of this animal was also within, rather than at one extreme of, the five rhesus animals (Figs. 4, 6).

We did not perform a formal assessment of reproducibility on the eyes in this study, and the slight differences we report may be within the variability of our measurements. However, we think this explanation is unlikely for most parameters for the following reasons: First, the intra- and interdelineator reproducibility of our parameters (Table 2) has been extensively characterized in a series of previous reports.[24–26] Second, close inspection of these data suggest that the range of intradelineator variability for most parameters is less than the PID*max* for each parameter[28] that was used as the criterion for EPID*max* change. Thus, we believe that for most parameters, our EPID*max* difference, when present, represented change beyond the variability due to delineation, had it been directly assessed in these eyes.

Finally, we chose to order our monkeys from 1 to 6 based on the regional change in the parameter post-NCO total prelaminar volume (Table 2 and Fig. 6) and the degree to which this change colocalized with EPID*max* changes in other parameters. When we used these criteria, monkeys 5 and 6 demonstrated the greatest amount of colocalized deformation. At present, there is no precise way to order the monkeys' deformation, and this choice may be arbitrary, as by other overall and regional measures other monkeys may have exceeded monkey 5. Our choice of this parameter reflects our underlying belief that there is a progression in the individual forms of deformation within these tissues that leads to their colocalization. At present, this is a hypothesis that should be studied in living eyes by using in vivo measures of ONH connective tissue deformation, as mentioned earlier.

Our results have the following implications. First, although the lamina demonstrated little anterior or posterior deformation, it did demonstrate regional thinning, in some cases colocalized with the greatest magnitude of canal expansion (monkey 6, Fig. 6). This point is important, because it emphasizes the difference between overall deformation of a biological structure (the lamina cribrosa) and local deformation (strain) within its component elements. Expansion of the scleral canal and the associated laminar thinning should result in expansion of the laminar pores and thinning and elongation of laminar beams. The effects on the contained laminar capillaries, astrocytes, and adjacent axons, as well as the transfer of nutrients between them, may be substantial. The thinning of the lamina cribrosa also increases the steepness of the translaminar pressure gradient [(IOP − retrolaminar tissue pressure)/laminar thickness] which may have separate implications for astrocyte physiology and retinal ganglion cell axoplasmic transport and flow.[15,16,68,70–75] Characterization of alterations in laminar beam microarchitecture[27,65] (Grimm J, et al. *IOVS* 2007;48:ARVO E-Abstract 3295) in these eyes, and the stresses and strains contained therein[76] (Kodiyalam S, et al. *IOVS* 2005;46:ARVO E-Abstract 1267), will also be the subject of future reports.

Second, although peripapillary scleral bowing and scleral canal expansion are likely to be important determinants of lamina cribrosa biomechanical behavior, their direct and indirect effects on axonal susceptibility within the ONH remain unclear. At a given perfusion pressure, bowing and thinning of the peripapillary sclera and laminar beams should influence blood flow within the contained laminar capillaries and posterior ciliary arteries, but these effects have yet to be determined.

Finally, our EPID*max* criteria for detecting postmortem change may be conservative. Within the regional data, in many instances, statistically significant differences did not achieve EPID*max* criteria and were not considered change. We believe the trends that are present in our data are important indicators of early viscoelastic deformation. This prediction is currently under study with in vivo SD-OCT imaging of the neural canal, lamina cribrosa, and peripapillary sclera after 30, 60, 90, and 120 minutes of IOP elevation in very young and very old monkey eyes (Burgoyne CF, et al. *IOVS* 2008;49:ARVO E-Abstract 3655).

Acknowledgments

The authors thank the following individuals for assistance during the study: Jonathon Grimm and Juan Reynaud for help with software for volumetric and thickness quantification; Galen Williams and Erica Dyrud for help with delineation; Pris Zhou and Anthony Bellezza, PhD, for directing the animal testing; Joanne Couchman for assistance with manuscript preparation; and Stuart Gardiner for statistical consultation.

References

1. Asai T, Katsumori N, Mizokami K. Retinal ganglion cell damage in human glaucoma. 2. Studies on damage pattern (in Japanese). *Nippon Ganka Gakkai Zasshi.* 1987;91:1204–1213.
2. Garcia-Valenzuela E, Shareef S, Walsh J, Sharma SC. Programmed cell death of retinal ganglion cells during experimental glaucoma. *Exp Eye Res.* 1995;61:33–44.
3. Quigley HA, Nickells RW, Kerrigan LA, Pease ME, Thibault DJ, Zack DJ. Retinal ganglion cell death in experimental glaucoma and after axotomy occurs by apoptosis. *Invest Ophthalmol Vis Sci.* 1995;36:774–786.
4. Weber AJ, Kaufman PL, Hubbard WC. Morphology of single ganglion cells in the glaucomatous primate retina. *Invest Ophthalmol Vis Sci.* 1998;39:2304–2320.
5. Quigley HA, McKinnon SJ, Zack DJ, et al. Retrograde axonal transport of BDNF in retinal ganglion cells is blocked by acute IOP elevation in rats. *Invest Ophthalmol Vis Sci.* 2000;41:3460–3466.
6. Quigley HA. Ganglion cell death in glaucoma: pathology recapitulates ontogeny. *Aust N Z J Ophthalmol.* 1995;23:85–91.
7. Wygnanski T, Desatnik H, Quigley HA, Glovinsky Y. Comparison of ganglion cell loss and cone loss in experimental glaucoma. *Am J Ophthalmol.* 1995;120:184–189.
8. Panda S, Jonas JB. Decreased photoreceptor count in human eyes with secondary angle-closure glaucoma. *Invest Ophthalmol Vis Sci.* 1992;33:2532–2536.
9. Kendell KR, Quigley HA, Kerrigan LA, Pease ME, Quigley EN. Primary open-angle glaucoma is not associated with photoreceptor loss. *Invest Ophthalmol Vis Sci.* 1995;36:200–205.
10. Nork TM, Ver Hoeve JN, Poulsen GL, et al. Swelling and loss of photoreceptors in chronic human and experimental glaucomas. *Arch Ophthalmol.* 2000;118:235–245.
11. Janssen P, Naskar R, Moore S, Thanos S, Thiel HJ. Evidence for glaucoma-induced horizontal cell alterations in the human retina. *Ger J Ophthalmol.* 1996;5:378–385.
12. Yucel YH, Zhang Q, Gupta N, Kaufman PL, Weinreb RN. Loss of neurons in magnocellular and parvocellular layers of the lateral geniculate nucleus in glaucoma. *Arch Ophthalmol.* 2000;118:378–384.
13. Yucel YH, Zhang Q, Weinreb RN, Kaufman PL, Gupta N. Atrophy of relay neurons in magno- and parvocellular layers in the lateral geniculate nucleus in experimental glaucoma. *Invest Ophthalmol Vis Sci.* 2001;42:3216–3222.
14. Yucel YH, Zhang Q, Weinreb RN, Kaufman PL, Gupta N. Effects of retinal ganglion cell loss on magno-, parvo-, koniocellular pathways in the lateral geniculate nucleus and visual cortex in glaucoma. *Prog Retin Eye Res.* 2003;22:465–481.
15. Gaasterland D, Tanishima T, Kuwabara T. Axoplasmic flow during chronic experimental glaucoma. 1. Light and electron microscopic studies of the monkey optic nervehead during development of glaucomatous cupping. *Invest Ophthalmol Vis Sci.* 1978;17:838–846.
16. Minckler DS, Bunt AH, Johanson GW. Orthograde and retrograde axoplasmic transport during acute ocular hypertension in the monkey. *Invest Ophthalmol Vis Sci.* 1977;16:426–441.

17. Quigley HA, Addicks EM, Green WR, Maumenee AE. Optic nerve damage in human glaucoma. II. The site of injury and susceptibility to damage. *Arch Ophthalmol.* 1981;99:635–649.
18. Quigley HA, Green WR. The histology of human glaucoma cupping and optic nerve damage: clinicopathologic correlation in 21 eyes. *Ophthalmology.* 1979;86:1803–1830.
19. Bellezza AJ, Rintalan CJ, Thompson HW, Downs JC, Hart RT, Burgoyne CF. Deformation of the lamina cribrosa and anterior scleral canal wall in early experimental glaucoma. *Invest Ophthalmol Vis Sci.* 2003;44:623–637.
20. Burgoyne CF, Downs JC, Bellezza AJ, Hart RT. Three-dimensional reconstruction of normal and early glaucoma monkey optic nerve head connective tissues. *Invest Ophthalmol Vis Sci.* 2004;45:4388–4399.
21. Yan DB, Coloma FM, Metheetrairut A, Trope GE, Heathcote JG, Ethier CR. Deformation of the lamina cribrosa by elevated intraocular pressure. *Br J Ophthalmol.* 1994;78:643–648.
22. Levy NS, Crapps EE. Displacement of optic nerve head in response to short-term intraocular pressure elevation in human eyes. *Arch Ophthalmol.* 1984;102:782–786.
23. Downs JC, Suh JK, Thomas KA, Bellezza AJ, Hart RT, Burgoyne CF. Viscoelastic material properties of the peripapillary sclera in normal and early-glaucoma monkey eyes. *Invest Ophthalmol Vis Sci.* 2005;46:540–546.
24. Downs JC, Yang H, Girkin C, et al. Three dimensional histomorphometry of the normal and early glaucomatous monkey optic nerve head: neural canal and subarachnoid space architecture. *Invest Ophthalmol Vis Sci.* 2007;48:3195–3208.
25. Yang H, Downs JC, Bellezza AJ, Thompson H, Burgoyne CF. 3-D Histomorphometry of the normal and early glaucomatous monkey optic nerve head: prelaminar neural tissues and cupping. *Invest Ophthalmol Vis Sci.* 2007;48:5068–5084.
26. Yang H, Downs JC, Girkin C, et al. 3-D Histomorphometry of the normal and early glaucomatous monkey optic nerve head: lamina cribrosa and peripapillary scleral position and thickness. *Invest Ophthalmol Vis Sci.* 2007;48:4597–4607.
27. Roberts MD, Grau V, Grimm J, et al. Remodeling of the connective tissue microarchitecture of the lamina cribrosa in early experimental glaucoma *Invest Ophthalmol Vis Sci*. 2009;50:681–690.
28. Yang H, Downs JC, Burgoyne CF. Physiologic intereye differences in monkey optic nerve head architecture and their relation to changes in early experimental glaucoma. *Invest Ophthalmol Vis Sci.* 2009;50:224–234.
29. Johnson EC, Morrison JC, Farrell S, Deppmeier L, Moore CG, McGinty MR. The effect of chronically elevated intraocular pressure on the rat optic nerve head extracellular matrix. *Exp Eye Res.* 1996;62:663–674.
30. Johnson EC, Deppmeier LM, Wentzien SK, Hsu I, Morrison JC. Chronology of optic nerve head and retinal responses to elevated intraocular pressure. *Invest Ophthalmol Vis Sci.* 2000;41:431–442.
31. Cepurna WO, Kayton RJ, Johnson EC, Morrison JC. Age related optic nerve axonal loss in adult Brown Norway rats. *Exp Eye Res.* 2005;80:877–884.
32. Howell GR, Libby RT, Jakobs TC, et al. Axons of retinal ganglion cells are insulted in the optic nerve early in DBA/2J glaucoma. *J Cell Biol.* 2007;179:1523–1537.
33. Burgoyne CF, Downs JC, Bellezza AJ, Suh JK, Hart RT. The optic nerve head as a biomechanical structure: a new paradigm for understanding the role of IOP-related stress and strain in the pathophysiology of glaucomatous optic nerve head damage. *Prog Retin Eye Res.* 2005;24:39–73.
34. Varela HJ, Hernandez MR. Astrocyte responses in human optic nerve head with primary open-angle glaucoma. *J Glaucoma.* 1997;6:303–313.
35. Hernandez MR, Pena JD, Selvidge JA, Salvador-Silva M, Yang P. Hydrostatic pressure stimulates synthesis of elastin in cultured optic nerve head astrocytes. *Glia.* 2000;32:122–136.
36. Hernandez MR. The optic nerve head in glaucoma: role of astrocytes in tissue remodeling. *Prog Retin Eye Res.* 2000;19:297–321.
37. Agapova OA, Yang P, Wang WH, et al. Altered expression of 3 alpha-hydroxysteroid dehydrogenases in human glaucomatous optic nerve head astrocytes. *Neurobiol Dis.* 2003;14:63–73.
38. Hernandez MR, Agapova OA, Yang P, Salvador-Silva M, Ricard CS, Aoi S. Differential gene expression in astrocytes from human normal and glaucomatous optic nerve head analyzed by cDNA microarray. *Glia.* 2002;38:45–64.
39. Brooks DE, Kallberg ME, Cannon RL, et al. Functional and structural analysis of the visual system in the rhesus monkey model of optic nerve head ischemia. *Invest Ophthalmol Vis Sci.* 2004;45:1830–1840.
40. Cioffi GA, Sullivan P. The effect of chronic ischemia on the primate optic nerve. *Eur J Ophthalmol.* 1999;9(suppl 1):S34–S36.
41. Cioffi GA, Wang L, Fortune B, et al. Chronic ischemia induces regional axonal damage in experimental primate optic neuropathy. *Arch Ophthalmol.* 2004;122:1517–1525.
42. Orgul S, Cioffi GA, Wilson DJ, Bacon DR, Van Buskirk EM. An endothelin-1 induced model of optic nerve ischemia in the rabbit. *Invest Ophthalmol Vis Sci.* 1996;37:1860–1869.
43. Investigators A. The Advanced Glaucoma Intervention Study (AGIS): 7. The relationship between control of intraocular pressure and visual field deterioration. *Am J Ophthalmol.* 2000;130:429–440.
44. Kass MA, Heuer DK, Higginbotham EJ, et al. The Ocular Hypertension Treatment Study: a randomized trial determines that topical ocular hypotensive medication delays or prevents the onset of primary open-angle glaucoma. *Arch Ophthalmol.* 2002;120:701–713.
45. Leske MC, Heijl A, Hussein M, Bengtsson B, Hyman L, Komaroff E. Factors for glaucoma progression and the effect of treatment: the early manifest glaucoma trial. *Arch Ophthalmol.* 2003;121:48–56.
46. Anderson DR, Drance SM, Schulzer M. Factors that predict the benefit of lowering intraocular pressure in normal tension glaucoma. *Am J Ophthalmol.* 2003;136:820–829.
47. Albon J, Purslow PP, Karwatowski WS, Easty DL. Age related compliance of the lamina cribrosa in human eyes. *Br J Ophthalmol.* 2000;84:318–323.
48. Bellezza AJ, Rintalan CJ, Thompson HW, Downs JC, Hart RT, Burgoyne CF. Anterior scleral canal geometry in pressurised (IOP 10) and non-pressurised (IOP 0) normal monkey eyes. *Br J Ophthalmol.* 2003;87:1284–1290.
49. Strouthidis NG, Yang H, Fortune B, Downs JC, Burgoyne CF. Detection of optic nerve head neural canal opening within histomorphometric and spectral domain optical coherence tomography data sets. *Invest Ophthalmol Vis Sci.* 2009;50:214–223.
50. Edwards D, Berry JJ. The efficiency of simulation-based multiple comparisons. *Biometrics.* 1987;43:913–928.
51. Sigal IA, Flanagan JG, Tertinegg I, Ethier CR. Modeling individual-specific human optic nerve head biomechanics. Part I: IOP-induced deformations and influence of geometry. *Biomech Model Mechanobiol.* 2009;8(2):85–98.
52. Downs JC, Suh JK, Thomas KA, Bellezza AJ, Burgoyne CF, Hart RT. Viscoelastic characterization of peripapillary sclera: material properties by quadrant in rabbit and monkey eyes. *J Biomech Eng.* 2003;125:124–131.
53. Sigal IA, Flanagan JG, Tertinegg I, Ethier CR. Reconstruction of human optic nerve heads for finite element modeling. *Technol Health Care.* 2005;13:313–329.
54. Sigal IA, Flanagan JG, Ethier CR. Factors influencing optic nerve head biomechanics. *Invest Ophthalmol Vis Sci.* 2005;46:4189–4199.
55. Sigal IA, Flanagan JG, Tertinegg I, Ethier CR. Finite element modeling of optic nerve head biomechanics. *Invest Ophthalmol Vis Sci.* 2004;45:4378–4387.
56. Sigal IA, Flanagan JG, Tertinegg I, Ethier CR. Modeling individual-specific human optic nerve head biomechanics. Part II: influence of material properties. *Biomech Model Mechanobiol.* 2009;8(2):99–109.
57. Girard MJ, Downs JC, Bottlang M, Burgoyne CF, Suh JK. Peripapillary and posterior scleral mechanics. Part II: experimental and inverse finite element characterization. *J Biomech Eng.* 2009;8(2):99–109.
58. Sigal IA. Interactions between geometry and mechanical properties on the optic nerve head. *Invest Ophthalmol Vis Sci.* 2009;50:2785–2795.

59. Srinivasan VJ, Adler DC, Chen Y, et al. Ultrahigh-speed optical coherence tomography for three-dimensional and en face imaging of the retina and optic nerve head. *Invest Ophthalmol Vis Sci.* 2008;49:5103–5110.
60. Kagemann L, Ishikawa H, Wollstein G, et al. Ultrahigh-resolution spectral domain optical coherence tomography imaging of the lamina cribrosa. *Ophthalmic Surg Lasers Imaging.* 2008;39:S126–S131.
61. Brown DJ, Morishige N, Neekhra A, Minckler DS, Jester JV. Application of second harmonic imaging microscopy to assess structural changes in optic nerve head structure ex vivo. *J Biomed Opt.* 2007;12:024029.
62. Greene PR, McMahon TA. Scleral creep vs. temperature and pressure in vitro. *Exp Eye Res.* 1979;29:527–537.
63. Phillips JR, Khalaj M, McBrien NA. Induced myopia associated with increased scleral creep in chick and tree shrew eyes. *Invest Ophthalmol Vis Sci.* 2000;41:2028–2034.
64. Roberts MD, Liang Y, Sigal IA, et al. Correlation between local stress and strain and lamina cribrosa connective tissue volume fraction in normal monkey eyes. *Invest Ophthalmol Vis Sci.* In press.
65. Roberts MD, Hart RT, Liang Y, Bellezza AJ, Burgoyne CF, Downs JC. *Continuum-Level Finite Element Modeling of the Optic Nerve Head Using a Fabric Tensor Based Description of the Lamina Cribrosa.* Presented at the ASME Summer Bioengineering Conference. Keystone, CO: American Society of Mechanical Engineers; 2007.
66. Burgoyne CF, Quigley HA, Thompson HW, Vitale S, Varma R. Measurement of optic disc compliance by digitized image analysis in the normal monkey eye. *Ophthalmology.* 1995;102:1790–1799.
67. Burgoyne CF, Quigley HA, Thompson HW, Vitale S, Varma R. Early changes in optic disc compliance and surface position in experimental glaucoma. *Ophthalmology.* 1995;102:1800–1809.
68. Morgan WH, Yu DY, Cooper RL, Alder VA, Cringle SJ, Constable IJ. The influence of cerebrospinal fluid pressure on the lamina cribrosa tissue pressure gradient. *Invest Ophthalmol Vis Sci.* 1995; 36:1163–1172.
69. Downs JC, Blidner RA, Bellezza AJ, Thompson HW, Hart RT, Burgoyne CF. Peripapillary scleral thickness in perfusion-fixed normal monkey eyes. *Invest Ophthalmol Vis Sci.* 2002;43:2229–2235.
70. Jonas JB, Berenshtein E, Holbach L. Anatomic relationship between lamina cribrosa, intraocular space, and cerebrospinal fluid space. *Invest Ophthalmol Vis Sci.* 2003;44:5189–5195.
71. Morgan WH, Yu DY, Balaratnasingam C. The role of cerebrospinal fluid pressure in glaucoma pathophysiology: the dark side of the optic disc. *J Glaucoma.* 2008;17:408–413.
72. Berdahl JP, Allingham RR, Johnson DH. Cerebrospinal fluid pressure is decreased in primary open-angle glaucoma. *Ophthalmology.* 2008;115:763–768.
73. Hollander H, Makarov F, Stefani FH, Stone J. Evidence of constriction of optic nerve axons at the lamina cribrosa in the normotensive eye in humans and other mammals. *Ophthalmic Res.* 1995; 27:296–309.
74. Quigley H, Anderson DR. The dynamics and location of axonal transport blockade by acute intraocular pressure elevation in primate optic nerve. *Invest Ophthalmol Vis Sci.* 1976;15:606–616.
75. Quigley HA, Anderson DR. Distribution of axonal transport blockade by acute intraocular pressure elevation in the primate optic nerve head. *Invest Ophthalmol Vis Sci.* 1977;16: 640–644.
76. Downs JC, Roberts MD, Burgoyne CF, Hart RT. *Finite Element Modeling of the Lamina Cribrosa Microarchitecture in the Normal and Early Glaucoma Monkey Optic Nerve Head.* ASME Summer Bioengineering Conference. Keystone, CO: American Society of Mechanical Engineers; 2007.